

To be appeared in the ApJ
Submitted 2004/11/23; Accepted 2005/01/28

Relative Evolutionary Time Scale of Hot Molecular Cores with Respect to Ultra Compact HII Regions

R. S. Furuya¹

Division of Physics, Mathematics, and Astronomy, California Institute of Technology

rsf@astro.caltech.edu

R. Cesaroni²

INAF, Osservatorio Astrofisico di Arcetri

cesa@arcetri.astro.it

S. Takahashi³

Department of Astronomical Science, Graduate University for Advanced Studies

satoko@nro.nao.ac.jp

M. Momose⁴

Institute of Astronomy and Planetary Science, Ibaraki University

momose@mx.ibaraki.ac.jp

L. Testi²

INAF, Osservatorio Astrofisico di Arcetri

lt@arcetri.astro.it

H. Shinnaga⁵

Caltech Submillimeter Observatory, California Institute of Technology

shinnaga@submm.caltech.edu

and

C. Codella²

INAF – Istituto di Radioastronomia, Sezione di Firenze

`codella@arcetri.astro.it`

ABSTRACT

Using the Owens Valley and Nobeyama Radio Observatory interferometers, we carried out an unbiased search for hot molecular cores and ultracompact (UC) H_{II} regions toward the high-mass star forming region G19.61–0.23. In addition, we performed 1.2 mm imaging with SIMBA, and retrieved 3.5 and 2 cm images from the VLA archive data base. The newly obtained 3 mm image brings information on a cluster of high-mass (proto)stars located in the innermost and densest part of the parsec scale clump detected in the 1.2 mm continuum. We identify a total of 10 high-mass young stellar objects: one hot core (HC) and 9 UC H_{II} regions, whose physical parameters are obtained from model fits to their continuum spectra. The ratio between the current and expected final radii of the UC H_{II} regions ranges from 0.3 to 0.9, which leaves the possibility that all O-B stars formed simultaneously. Under the opposite assumption — namely that star formation occurred randomly — we estimate that HC lifetime is less than $\sim 1/3$ of that of UC H_{II} regions on the basis of the source number ratio between them.

Subject headings: H_{II} regions — ISM: evolution — ISM: individual (G19.61–0.23) — stars: early type — radio continuum: ISM

1. Introduction

It is widely accepted that high-mass stars ($> 8M_{\odot}$) form in clusters. However, identification of cluster members is complicated because zero-age main-sequence stars and high-mass protostars are deeply embedded in their molecular surroundings. It is hence impossible to

¹1201 East California Boulevard, Pasadena, CA 91125

²Largo Enrico Fermi 5, I-50125 Firenze, Italy

³Nobeyama Radio Observatory, Nobeyama 411, Minamimaki, Minamisaku, Nagano 384-1305, Japan

⁴Bunkyo 2-1-1, Mito, Ibaraki 310-8512, Japan

⁵111 North A'ohoku Place, Hilo, HI 96720

use a simple SED classification analogous to that applied to low-mass young stellar objects (YSOs). In this context, ultracompact (UC) ($\lesssim 0.1$ pc) H_{II} regions and hot cores (HCs) play a fundamental role (e.g., Kurtz et al. 2000). The former are very young H_{II} regions ionized by an O-B star which is embedded in the natal cloud. The latter are dense, hot, compact molecular cores which host even younger (proto)stars, although their life time has not been established. A comparison between the estimated number of UC H_{II} regions in the Galaxy and the O-B star formation rate yields a duration for the ultracompact phase of $\sim 10^5$ years (Wood & Churchwell 1989 [hereafter WC89]) which is two orders of magnitude larger than expected from the classical expansion model for H_{II} regions (e.g., Spitzer 1978). Several models have been proposed to explain this discrepancy (e.g., Akeson & Carlstrom 1996, and references therein). Clearly, one must have better knowledge of properties of clusters to which HC_s and UC H_{II} regions belong and of their natal molecular clumps.

A well-studied example of high-mass (proto)star cluster is W49N (at a distance of 11.4 kpc). Subsequent to the identification of 12 UC H_{II} regions powered by O stars (De Pree et al. 2000), Wilner et al. (2001) identified 6 HC_s from an unbiased survey of line and 1.4-mm continuum emission. Using the HC to UCH_{II} region number ratio, they obtained an estimate of 25–100% for the lifetime ratio between the HC and UC H_{II} region phases. However, the W49N study has an important limitation that the region is very distant which sets limits on the census of detectable YSOs. The high-mass star forming region G19.61–0.23 is an excellent target for a study of cluster formation because of its distance ($d = 3.5$ kpc; Churchwell, Walmsley, & Cesaroni 1990), and potential richness in terms of YSOs as indicated by studies at cm (e.g., Garay, Reid, & Moran 1985 [hereafter GRM85]; WC89; Garay et al. 1998; Forster & Caswell 2000) and mid-infrared (MIR) (De Buizer et al. 2003) wavelengths. In this letter, we present a study of the cm continuum emission with higher sensitivity and better angular resolution, complemented by mm wavelength observations.

2. Observations and Archive Data Retrieval

Aperture synthesis observations at 3 mm were carried out using Owens Valley Radio Observatory (OVRO) millimeter array and Nobeyama¹ Millimeter Array (NMA) with a total of 6 array configurations in the period from 2002 December till 2004 April. More than 15 molecular lines (R. Furuya et al. in preparation) were observed simultaneously with the continuum emission at 89.9 GHz. The flux density of the calibrator was bootstrapped from

¹Nobeyama Radio Observatory is a branch of the National Astronomical Observatory, operated by the Ministry of Education, Culture, Sports, Science and Technology, Japan.

planets with an uncertainty of 15%. Combining the continuum data from both arrays, we obtain a synthesized beam of $1''.52 \times 1''.51$, and an RMS noise level of $2.8 \text{ mJy beam}^{-1}$.

On 2003 July 29, we used the SIMBA bolometer array on the SEST 15-m telescope to obtain a parsec-scale map ($3.0' \times 4.0'$ in size) of 1.2 mm continuum emission. Observing η Carinae and Uranus, we checked pointing accuracy ($\text{RMS} \simeq 2''$), and made flux calibrations.

We retrieved 3.5 and 2 cm data from the archive of the NRAO² Very Large Array (VLA). The 3.5 cm data were taken from projects AW374A and AK470 (A-array), AK470 (B), AK423 (CnB), and AK450 (D), and the 2 cm data from AW158 (B and C), AK423 (CnB). Resulting beam sizes and noise levels are $0''.33 \times 0''.23$ and $0''.55 \times 0''.50$ with 0.31 and 1.7 mJy beam $^{-1}$ at 3.5 and 2 cm, respectively.

3. Results and Analysis

Figure 1 presents the SIMBA 1.2 mm continuum emission map where two clumps separated by $\sim 75''$ (i.e. 1.3 pc) are seen over a region of $\sim 4.1 \text{ pc} \times 1.7 \text{ pc}$. The brighter clump to the west hosts the G19.61–0.23 complex. A total flux density (S_ν) of 19.4 Jy is obtained by integrating the emission inside the 3σ contour level. Figure 2a shows the VLA image of the 3.5 cm continuum emission toward the center of the western clump, where a cometary shaped and several compact HII regions, surrounded by a 0.1-pc halo, are seen.

Since the minimum projected baseline lengths (0.78, 7.7, and $2.8 \text{ k}\lambda$ for the 3.5, 2 cm, and 3 mm data, respectively) and beam sizes (§2) are not identical, we reconstructed all the interferometric images with a $1''.5$ beam using visibilities with a uv -radius greater than $7.7 \text{ k}\lambda$. This makes our images insensitive to structures more extended than $27''$ (i.e. 0.46 pc). Thus only the 0.1-pc halo common to all of the cluster members is resolved out. Figure 2b represents an overlay of such maps at 3.5, 2 cm and 3 mm. Most of the 3 mm peaks are associated with previously identified cm sources (GRM85; WC89; Garay et al. 1998), suggesting that our 3 mm map is sensitive to both free-free emission from ionized gas inside the compact HII regions and thermal emission from dust grains in the surrounding cores. To establish the properties of the dust continuum emission, we need to remove the free-free emission from the 3 mm map. We produced a “pure” free-free emission image at 3 mm by extrapolating the 3.5 cm map assuming optically thin emission ($I_\nu \propto \nu^{-0.1}$). Then we subtracted this from the 3 mm continuum image, thus obtaining a “pure” dust emission

²The National Radio Astronomy Observatory is a facility of the National Science Foundation operated under cooperative agreement by Associated Universities, Inc.

map (see Figure 2c). Taking into account the calibration errors at the various wavelengths, we estimate a subtraction uncertainty of 4.3 mJy beam $^{-1}$. The resulting map presents a strong (29σ) peak lying between the UC H II regions labeled A and C (see the yellow cross in Figure 2a), where no emission peak is seen in 2 and 3.5 cm images. Instead, the 3 mm peak coincides with a molecular core (Figure 2d) detected in the CH₃CH₂CN (11–10) and SO₂ (8_{3,5} – 9_{2,8}) lines: these molecular species are typical tracers of HCs (van Dishoeck & Blake 1998). The core is also traced by other molecules such as NH₃ (Garay et al. 1998), CH₃CN (Kurtz et al. 2000), HCOOCH₃, H¹³CN, HN¹³C, H¹³CO⁺, and SO (R. Furuya et al. in preparation). Such a richness in molecular species makes this core very similar to Orion-KL (Wright, Plambeck, & Wilner 1996) and other HCs (Kurtz et al. 2000). In addition, the presence of H₂O (Hofner & Churchwell 1996) and OH (GRM85) masers strongly suggest that the (proto)star deeply embedded in the core is too young to ionize its surrounding material because masers are believed to disappear during the development of an UC H II region. No other prominent “dust” condensation was detected above a 5σ upper limit of 21.5 mJy beam $^{-1}$, although extended emission is seen towards some of the H II regions. Such an upper limit corresponds to a sensitivity in gas plus dust mass of $27 M_{\odot}$ beam $^{-1}$ for a typical HC temperature of 100 K (Kurtz et al. 2000). The large majority ($\sim 85\%$) of the HCs known to date (e.g. Table 1 of Kurtz et al. 2000) are above this limit, but we cannot rule out the possibility to have missed the least massive ones ($\sim 10 M_{\odot}$).

We have identified the UC H II regions in the cluster with a procedure, which iteratively fitted and subtracted prominent emission peaks from the cm maps, until the signal in the residual image was below 5σ . The borders of the cometary shaped UC H II region A and the source J at 2 cm were identified as the 5σ contour levels enclosing them, whereas for all the other UC H II regions a 2-D gaussian fit was used. This gave us the peak position, S_{ν} , and deconvolved source diameter of the sources. In the estimate of the error on S_{ν} , we considered the formal error of the fit, the flux calibration uncertainty, and the contribution due to the noise in the map. In this way, we identified 9 UC H II regions, labeled A–D, F, G, I, J, and K. All of these were identified both at 3.5 and 2 cm, with the sole exception of J, too faint to be detected in the 2 cm image.

In order to derive the properties of the UC H II regions at 3 mm, it was necessary to disentangle the HC from UC H II regions A and C. For this purpose, we used the free-free subtracted map at 3 mm (Figure 2c) to fit the HC with a 2-D Gaussian. Then this gaussian model was subtracted from the original 3 mm image. The resulting “clean” image was treated in the same way as the 3.5 and 2 cm maps to identify the counterparts of the cm sources. Because of the difficulty to define unique area for object F at 3 mm, we estimate an uncertainty equal to the difference between the flux estimate obtained from Gaussian fitting and that from integrating the emission inside the 5σ contour. In Figures 2b and c,

one can see that an isolated 3 mm source lies to the east of A: we assume that this emission is associated with the tail of the cometary UC H_{II} region A rather than to a distinct YSO. We thus identified 6 objects at 3 mm, including the HC, above a detection threshold of 5σ . In conclusion, we have identified a total of 10 high-mass YSOs: 1 HC and 9 UC H_{II} regions (Table 1). Note that we detected all the radio sources previously identified by other authors, except source E of WC89. All 9 UC H_{II} regions have been detected at more than 2 bands at cm wavelengths, if one takes into account identifications reported in the literature.

4. Discussion

We analyzed the continuum spectra of the whole region and of each cluster member by modeling the emission as originating from a dust-free H_{II} region surrounded by a dusty molecular shell. Spherical symmetry and homogeneity are assumed for both the H_{II} region and the shell. The spectrum of the whole region is shown in Figure 106 of WC89. To the data reported in this figure we have added our fluxes at 3 and 1.2 mm (§3), and that at 350 μ m by Mueller et al. (2002). Most of the 3 mm emission is due to free-free, while the emission shortward of 1.2 mm is originating from dust. Given the complexity of the region seen in free-free emission, we estimate only a pc-scale mean dust temperature (T_d) and a total mass of the gas plus dust (M_d). Therefore, the contribution of the H_{II} region was considered only to subtract the free-free component from the spectrum. We adopted a dust absorption coefficient $\kappa_\nu = \kappa_0 (\nu/\nu_0)^\beta$ with $\kappa_0=0.005 \text{ cm}^2 \text{ g}^{-1}$ at $\nu_0=230 \text{ GHz}$ (Preibish et al. 1993) and $\beta=1.5$. We obtain $T_d \approx 42 \text{ K}$, and $M_d \approx 2800 \pm 100 M_\odot$, which are very similar to the values of other clumps containing high-mass YSOs (e.g. Fontani et al. 2002, and references therein).

Subsequently we have analyzed the continuum spectra of the 10 sources in the cluster using the above model. In the fits we fixed radii of H_{II} regions (R_{HII}) and dusty shells (R_d) to the values derived respectively from the 3.5 cm and 3 mm maps, and the electron temperatures (T_e) to those obtained from recombination line observations (Garay et al. 1998). For source A at the 3 bands, D and F at 3 mm, and J at 2 cm, we defined an effective radius as that of a circle with the same area as the UC H_{II} region or the dusty shell. We assumed a mean T_e of 7200 K for the objects where T_e are not available in Table 5 of Garay et al. 1998. Therefore, free parameters were the emission measure (EM) of the H_{II} region, and M_d and T_d of the dusty molecular shell. Our spectral analysis shows that fluxes at 3 mm (Table 1), 20.8, 18.1, and 11.7 μ m (De Buizer et al. 2003) towards objects B, F, I, and the HC are fitted with combinations of thermal dust plus free-free emission, implying that they are likely to be embedded in dust cocoons. Only the HC is not detected at cm

wavelengths, which indicates that the putative embedded stars (or star) are too young or not massive enough to develop an UC H_{II} region. We favor the idea that the HC contains very young massive (proto)star(s) as it is in all aspects (richness of the molecular composition, large mass of 800 M_{\odot} , high temperature of 65 K) similar to the other HCs known in the literature, which are believed to be the cradle of early-type stars (Kurtz et al. 2000). If the HC contains a deeply embedded O-B star, one may estimate the maximum radius of the associated H_{II} region from the sensitivity of the 3.5 cm image. Assuming that the free-free emission is optically thick, such a radius must be smaller than 2.4×10^{-3} pc. The continuum spectrum of D is rising from cm wavelengths to 3 mm (Table 1), but does not show MIR emission. This sets upper limits on T_d and M_d . The 3 mm flux of source A (589±115 mJy) is only marginally above the value expected (409 mJy) from extrapolation of the free-free cm fluxes. Considering the uncertainties and the fact that its effective R_d is smaller than that of R_{HII} , we believe that thermal dust emission is not dominant at 3 mm. Finally, the spectrum of sources C, G, J, and K can be fitted with free-free emission only, suggesting that they have already dispersed most of the surrounding material.

An unbiased survey such as ours could be used to estimate the lifetime of HCs with respect to that of UC H_{II} regions on the basis of number ratio between the two. However, this applies only to a series of star formation episodes randomly distributed in time, and not if one is observing the result of a coherent burst of star formation (e.g. Welch et al. 1987). While in the former case the different numbers of sources in different evolutionary stages would be directly related to the time spent in each phase, in the latter hypothesis such numbers would be determined by the local physical conditions around individual stars. It is hence important to find out whether the ages of our sources are spread over a sufficiently large time interval or all very similar.

Naively, one might expect that the age of an H_{II} region is strictly related to its diameter. However the correspondence between size and age is still matter of debate. Nevertheless, in most expansion models of an H_{II} region is related only to the spectral type of the star and to the properties of the surrounding environment. It is hence reasonable to assume that the expansion will come to an end when pressure equilibrium is reached between the ionized and the surrounding molecular gas. As illustrated by De Pree, Goss, & Gaume (1998), their eqs. (4) and (7) give the final H_{II} region radius ($R_{\text{HII}}^{\text{final}}$) as a function of the stellar Lyman continuum photons, T_e , and the density and temperature of the molecular gas. Here we derived spectral types of B0 for A, B0.5 for B-D, F, G, I, K, and B1 for J. The value of $R_{\text{HII}}^{\text{final}}$ should be compared to the current UC H_{II} radius measured from the maps. Although it is impossible to obtain an “absolute” estimate of the age, ratios of $R_{\text{HII}}/R_{\text{HII}}^{\text{final}}$ may be used to estimate “relative” ages of UC H_{II} regions, with lower ratios corresponding to younger objects. To compute $R_{\text{HII}}^{\text{final}}$, we used the corresponding values of T_e and T_d , and a mean

density derived from the SIMBA observations ($\sim 3 \times 10^6 \text{ cm}^{-3}$). The ratio ranges from 0.3 to 0.9 (see Table 1). If the UC H_{II} regions have not yet reached pressure equilibrium with the surrounding cloud, such a ratio seems to indicate that they are in similar evolutionary stages, thus supporting the “starburst” scenario.

However, several caveats are in order: the density of molecular gas may vary over the natal cloud and the Lyman continuum of the stars may have been underestimated because of optically thick free-free emission and dust absorption inside the H_{II} region. This may easily introduce an uncertainty of an order of magnitude on $R_{\text{HII}}^{\text{final}}$ thus making the “starburst” hypothesis questionable. In fact, the expansion timescales obtained from eq. (3) of De Pree, Goss, & Gaume (1998) span a small range (120–480 yr), suggesting that the UC H_{II} regions are close to pressure equilibrium. It is hence worth considering also the opposite scenario, and take the number ratio between HCs and UC H_{II} regions as an estimate of their relative lifetimes.

Considering Poisson statistical errors, the number of HCs and UC H_{II} regions are respectively 1 ± 1 and 9 ± 3 , so that their ratio is $11_{-11}^{+22}\%$. This implies that the HC phase (τ_{HC}) should last less than $\sim 1/3$ of the UC H_{II} region phase (τ_{HII}), with a probability of 4% that the ratio exceeds this value. This conclusion seems to differ from that inferred for the O-star cluster in W49N (Wilner et al. 2001), where $\tau_{\text{HC}}/\tau_{\text{HII}} \simeq 25\text{--}100\%$. The two results could indicate that $\tau_{\text{HII}} \simeq 3\text{--}4 \tau_{\text{HC}}$. Alternatively, the difference might be easily explained in the “starburst” scenario, where the ratio between HCs and UC H_{II} regions depends on the environment around each star. Finally, another caveat is in order. Our statistics might be affected by the limited sensitivity of our 3 mm map. As previously explained, we are sensitive to HCs with masses in excess of $\sim 27 M_{\odot}$, whereas at cm wavelengths we detect stars earlier than B1. If O stars are born in massive HCs and B stars in lower mass HCs, our comparison between UC H_{II} regions around B stars and HCs hiding O stars is bound to be unreliable. More numerous and sensitive interferometric observations of O-B star clusters will be needed to improve the statistics.

The authors gratefully acknowledge an anonymous referee whose comments significantly improved the quality of the paper. R. S. F. thanks Prof. A. I. Sargent and J. M. Carpenter for critical readings of the manuscript and encouragement, M. Nielbock and L. Haikala for their generous help at SIMBA observations and data reduction. Many thanks are due also to T. Saito for his early contribution to this study, and to the staff at OVRO, NRO, NRAO, and SEST. Research at the Owens Valley Radio Observatory is supported by the National Science Foundation through NSF grant AST 02-28955.

REFERENCES

Akeson, R. L. & Carlstrom, J. E. 1996, *ApJ*, 470, 528

Cesaroni, R., Felli, M., Jenness, T., Neri, R., Olmi, L., Robberto, M., Testi, L., & Walmsley, C. M. 1999, *A&A*, 345, 949

Churchwell, E., Walmsley, C. M., & Cesaroni, R. 1990, *A&AS*, 83, 119

De Buizer, J. M., Radomski, J. T., Telesco, C. M., & Piña, R. K. 2003, *ApJ*, 598, 1127

De Pree, C. G., Goss, W. M., & Gaume, R. A. 1998, *ApJ*, 500, 847

De Pree, C. G., Wilner, D. J., Goss, W. M., Welch, W. J., & McGrath, E. 2000, *ApJ*, 540, 308

Fontani, F., Cesaroni, R., Caselli, P., & Olmi, L. 2002, *A&A*, 389, 603

Forster, J. R. & Caswell, J. L. 2000, *ApJ*, 530, 371

Garay, G., Reid, M. J., & Moran, J. M. 1985, *ApJ*, 289, 681 (GRM85)

Garay, G., Moran, J. M., Rodriguez, L. F., & Reid, M. J. 1998, *ApJ*, 492, 635

Hofner, P. & Churchwell, E. 1996, *A&AS*, 120, 283

Kurtz, S., Cesaroni, R., Churchwell, E., Hofner, P., & Walmsley, C. M. 2000, in *Protostars and Planets IV*, ed. V. Mannings, A. Boss, & S. Russell (Tucson: Univ. Arizona Press), 299

Mueller, K. E., Shirley, Y. L., Evans, N. J., & Jacobson, H. R. 2002, *ApJS*, 143, 469

Preibisch, T., Ossenkopf, V., Yorke, H. W., & Henning, T. 1993, *A&A*, 279, 577

Spitzer, L. 1978, *Physical Processes in the Interstellar Medium* (New York: Wiley-Interscience)

van Dishoeck, E. F. & Blake, G. A. 1998, *ARA&A*, 36, 317

Welch, W. J., Dreher, J. W., Jackson, J. M., Terebey, S., & Vogel, S. N. 1987, *Science*, 238, 1550

Wilner, D. J., De Pree, C. G., Welch, W. J., & Goss, W. M. 2001, *ApJ*, 550, L81

Wood, D. O. S. & Churchwell, E. 1989, *ApJ*, 340, 265 (WC89)

Wright, M. C. H., Plambeck, R. L., & Wilner, D. J. 1996, ApJ, 469, 216

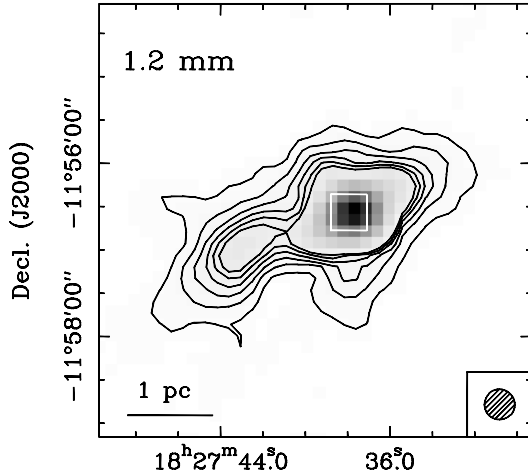


Fig. 1.— Parsec scale view of the cloud hosting the G19.61–0.23 region in 1.2 mm continuum emission. Contours start from the 3σ level of noise level ($30.7 \text{ mJy beam}^{-1}$), and end at the 15σ level with 3σ steps. The hatched ellipse in the bottom right corner indicates the SIMBA beam size (22''), and the central white box marks the region shown in Figure 2.

Fig. 2.— (a) 3.5 cm continuum emission map taken with VLA. The hatched ellipse in the bottom right corner indicates the beam size. The white contour corresponds to the 10σ level. The yellow cross indicates the position of the *dust* continuum emission peak (R.A. = $18^{\text{h}}27^{\text{m}}38^{\text{s}}066$, Decl. = $-11^{\circ} 56' 37''20$ in J2000). (b) Overlay of 3 mm continuum emission map taken with OVRO and NMA (grey scale plus black contour) on the 3.5 cm (**thick** purple contours) and 2 cm (thin green contours) maps CLEANed with the 3 mm beam (see text). The labels denote identified sources. Contour levels for the 3 mm map are 5σ intervals starting from the 5σ level ($\sigma_{3\text{mm}} = 4.3 \text{ mJy beam}^{-1}$). For the sake of clarity, we plot only 5σ , 10σ , and 30σ levels for the 3.5 cm map, and 5σ , 10σ , 20σ , and 40σ levels for the 2 cm map, where $\sigma = 0.38$ and $1.6 \text{ mJy beam}^{-1}$, respectively. (c) “Pure” *dust* continuum emission map obtained after subtraction from the 3 mm image of the 3.5 cm map suitably scaled to 3 mm (see text). Contours start from the 5σ level with a 5σ step ($\sigma_{dust} = 4.3 \text{ mJy beam}^{-1}$). (d) Overlay of total integrated intensity maps of $\text{CH}_3\text{CH}_2\text{CN}$ (11–10) (grey scale) and SO_2 $8_{3,5} - 9_{2,8}$ emission (green contours) taken with the NMA. Both the grey scale and green contours start from the 5σ level with 5σ steps, where noise levels and beam sizes are $14.1 \text{ mJy beam}^{-1}$ and $6''.40 \times 3''.65$ for $\text{CH}_3\text{CH}_2\text{CN}$, and $9.4 \text{ mJy beam}^{-1}$ and $4''.59 \times 2''.95$ for SO_2 . The open red circles and 6 blue triangles indicate the positions of the OH (GRM85), and H_2O (Hofner and Churchwell 1996) maser spots, respectively. The yellow cross has the same meaning as in (a).

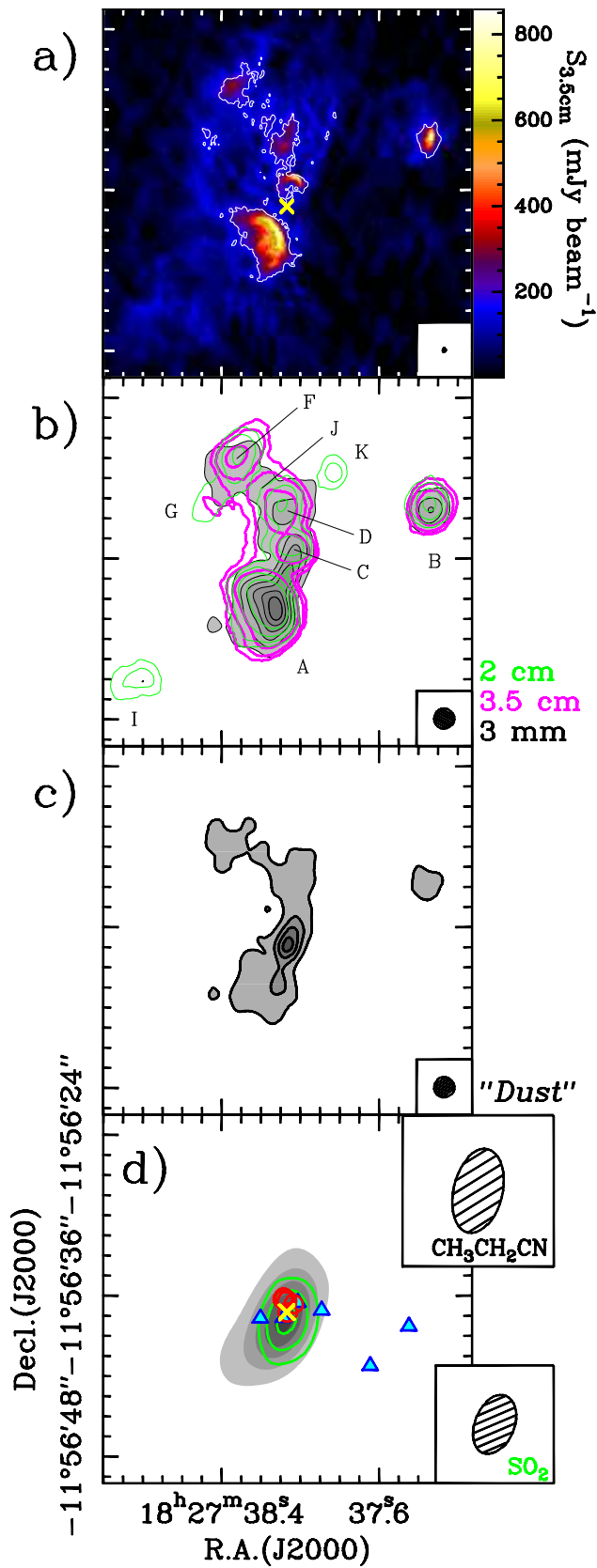


Table 1. Parameters of Identified Sources

YSO Name ^a				$S_{8.43}^{\text{b}}$	$S_{14.9}^{\text{b}}$	$S_{89.9}^{\text{b}}$	$R_{\text{HII}}^{\text{c}}$	EM	R_d	T_d	M_d	$R_{\text{HII}}/R_{\text{HII}}^{\text{final}}$
WC89	G98	D03		(mJy)	(mJy)	(mJy)	(pc)	(pc cm $^{-6}$)	(pc)	(K)	(M_{\odot})	
A	A	A	3	442 \pm 88	521 \pm 104	589 \pm 115	5.2E -2^{d}	1.3E $+7$	4.5E -2^{d}	70	760	0.8
B	B	B	2	72 $^{+16}_{-21}$	62 $^{+15}_{-12}$	201 $^{+40}_{-73}$	7.8E -3	8.3E $+7$	2.0E -2	70	400	0.3
C	C	F		52 \pm 10	50 $^{+38}_{-10}$	56 $^{+26}_{-11}$	1.2E -2	2.5E $+7$	0.4
D	D			68 $^{+14}_{-20}$	49 $^{+40}_{-10}$	187 $^{+37}_{-48}$	2.0E -2	1.2E $+7$	3.2E -2^{d}	< 70 ^e	< 580 ^e	0.6
F		CD	4	68 $^{+72}_{-33}$	57 $^{+29}_{-11}$	153 $^{+31}_{-46}$	1.7E -2	1.5E $+7$	2.7E -2^{d}	70	480	0.6
G				5.0 \pm 1	24 $^{+6}_{-7}$	< 17 ^e	2.0E -2	4.4E $+6$	0.8
HC				< 1.8	< 6.0	147 \pm 29	< 2.4E -3^{f}	...	1.7E -2	65	800	...
I		E	5	(4.7 $^{+1}_{-3}$)	43 $^{+22}_{-9}$	(21 \pm 4)	2.2E -2	6.3E $+6$	\sim 3E -2^{g} (70)	(35)	–	
J		CD ^h		5.2 \pm 1	< 6.0	< 17	1.2E -2^{d}	2.5E $+6$	0.9
K	D ^h			< 1.8	17 $^{+7}_{-3}$	< 17	2.2E -2	2.5E $+6$	–

^aFrom the left, source labels identified in this work, WC89, Garay et al.(1998), and De Buizer et al. (2003).

^bFlux densities are measured with a 1''.5 beam and a minimum projected baseline length of 7.7 $k\lambda$ (§3), and those in parenthesis are marginal detections that the significance levels of the peak intensities range between $\geq 3\sigma$ and $< 5\sigma$. All the results in the following analysis based on the marginal detections are shown in parenthesis. Upper limits are calculated with the 10σ level noise levels over the 1''.5 beam.

^cMeasured at 14.9 GHz for the sources I, G, and K.

^dEffective radius (§4)

^eUpper limit is from lack of well-defined emission peak at the 18.1 μm map (Figure 8 of De Buizer et al. 2003)

^fAssuming optically thick free-free emission (§4)

^gObtained from the 18.1 μm map (Figure 8 of De Buizer et al. 2003)

^hThe source J is located inside a circle given by the position of the source CD in G98 and its angular size (see their Table 2). The source K corresponds to the north-western peak of the 6 cm source D of WC89.